



# Impact of temperature on the role of Criegee intermediates and peroxy radicals in dimers formation from $\beta$ -pinene ozonolysis

Yiwei Gong<sup>1,2</sup>, Feng Jiang<sup>2</sup>, Yanxia Li,<sup>2</sup> Thomas Leisner<sup>2,3</sup>, and Harald Saathoff<sup>2</sup>

<sup>1</sup>Department of Atmospheric and Oceanic Sciences, School of Physics, Peking University, Beijing, China

<sup>2</sup>Institute of Meteorology and Climate Research, Karlsruhe Institute of Technology, Karlsruhe, Germany

<sup>3</sup>Institute of Environmental Physics, Heidelberg University, Heidelberg, Germany

Correspondence to: Yiwei Gong (yiwei.gong@kit.edu) and Harald Saathoff (harald.saathoff@kit.edu)

**Abstract.** Stabilized Criegee intermediates (SCIs) and organic peroxy radicals ( $\text{RO}_2$ ), as important reactive species in the atmosphere, are critical in oxidation processes and secondary organic aerosol (SOA) formation. However, the influence of temperature on these reactive intermediates and the corresponding reaction mechanisms in SOA formation are still not well defined. In this study, through utilizing SCIs scavengers and regulating  $[\text{HO}_2]/[\text{RO}_2]$  from  $\sim 0.3$  to  $\sim 1.9$ , the roles of  $\text{RO}_2$  and SCIs in SOA formation were investigated at 298 K, 273 K, and 248 K, respectively, particularly for dimers formation in  $\beta$ -pinene ozonolysis. The SOA yield increased by 21% from 298 K to 273 K, while further reducing the temperature to 248 K led to a decrease of 40% in SOA yield. This cannot be explained by partitioning or wall losses and is attributed to the temperature impact on rate coefficients and product branching ratios of some specific reactions. Both changing  $[\text{HO}_2]/[\text{RO}_2]$  and scavenging SCIs significantly affect SOA yield and composition. SCIs reactions accounted for more than 40% of dimers and SOA mass formation for all temperatures, and the dimers formed from the SCIs channel did not show obvious suppression at subzero temperature. Increasing  $[\text{HO}_2]/[\text{RO}_2]$  inhibited dimers and SOA formation with a higher sensitivity at lower temperatures. Compared to low  $[\text{HO}_2]/[\text{RO}_2]$  condition, the dimers abundance at high  $[\text{HO}_2]/[\text{RO}_2]$  decreased by about 31% at 298 K and 70% at 248 K. The correlation between dimers and  $[\text{RO}_2]^2$  demonstrates that  $\text{RO}_2$  cross reactions cannot explain the impact of  $\text{RO}_2$  concentration on dimers formation at low temperatures. The specific impact of  $[\text{HO}_2]/[\text{RO}_2]$  on SCIs-controlled dimers at lower temperatures indicates the influence of changing  $[\text{HO}_2]/[\text{RO}_2]$  on dimers formed from the reaction of  $\text{C}_9$ -SCIs and  $\text{RO}_2$  with a negative temperature dependence. The higher contribution of this SCIs reaction channel to dimers at lower temperatures is confirmed by chemical kinetic modeling. The dimers formed from  $\text{C}_9$ -SCIs reaction with  $\text{RO}_2$  were estimated to decrease by 61% at high  $[\text{HO}_2]/[\text{RO}_2]$  compared to low  $[\text{HO}_2]/[\text{RO}_2]$  at 248 K, providing explanations for the observed  $[\text{HO}_2]/[\text{RO}_2]$  impact. The high reactivity and substantial contribution to SOA of  $\beta$ -pinene-derived SCIs at lower temperatures observed in this study suggest that monoterpene-derived SCIs reactions should be accounted for in describing colder regions of the atmosphere.

## 1 Introduction

Secondary organic aerosols (SOA) have received considerable attention over the past decades due to their critical role in air quality and climate change (Hallquist et al., 2009; Kanakidou et al., 2005). Although significant progress has been made in understanding and modelling SOA formation and composition, the impact of temperature on the mechanism of SOA formation is still not well understood, especially for colder conditions ( $\leq 0$  °C) (Porter et al., 2021). Several studies investigated SOA yields of monoterpene oxidation at different temperatures, and they usually reported higher yields for lower temperatures (Jonsson et al., 2008; Pathak et al., 2007, 2008; Saathoff et al., 2009). Some studies reported a reduced formation of dimers and highly oxygenated molecules (HOMs) for lower temperatures, both of which are important SOA constituents, suggesting that besides the volatility of the particulate compounds, temperature also impacts the chemical reaction mechanisms (Kristensen et al., 2017; Simon et al., 2020). As for now, limited attention has been paid to how the temperature would impact



the reaction mechanisms of reactive intermediates in the atmosphere, such as stabilized Criegee intermediates (SCIs) and  
40 organic peroxy radicals (RO<sub>2</sub>), and their performances in SOA formation.

It has been proven that SCIs and RO<sub>2</sub> can react with other trace gas species and generate semi-volatile organic compounds (SVOCs) and low-volatile organic compounds (LVOCs) (Chhantyal-Pun et al., 2020a; Orlando and Tyndall, 2012). The structural diversity, short lifetime, and low concentration of SCIs and RO<sub>2</sub> make it challenging to study their fate in the atmosphere. SCIs, formed from alkene ozonolysis, perform as an efficient oxidant for several trace species, contributing to the  
45 formation of inorganic and organic aerosol components (Cox et al., 2020; Percival et al., 2013). SCIs' reaction properties are structure-dependent, and although many researches have synthesized and studied simple SCIs containing ≤ 3 carbon atoms, the reactivities of larger SCIs, such as monoterpene-derived and sesquiterpene-derived SCIs, are still vague (Lin and Chao, 2017). The bimolecular reactions of simple SCIs with SO<sub>2</sub>, carbonyl compounds, and water dimers have negative temperature dependences (Chhantyal-Pun et al., 2017; Onel et al., 2021; Smith et al., 2015; Wang et al., 2022). Lower temperatures could  
50 significantly promote the stabilization of SCIs and reduce the unimolecular decay rate of SCIs (Peltola et al., 2020; Robinson et al., 2022; Smith et al., 2016). Would this lead to a more important role of SCIs in SOA formation in winter and colder regions of the atmosphere? RO<sub>2</sub> radicals are vital in the atmospheric radical circle, and reactions with HO<sub>2</sub>, RO<sub>2</sub>, and NO are the main reaction pathways of RO<sub>2</sub> in the atmosphere. The reactions with HO<sub>2</sub> and RO<sub>2</sub> are important for determining the fate of RO<sub>2</sub> in clean areas and urban areas with NO reduction. In recent years, autoxidation has been claimed to be a competitive  
55 reaction pathway for RO<sub>2</sub> radicals with a positive temperature dependence (Praske et al., 2017). The rate coefficient of RO<sub>2</sub>+HO<sub>2</sub> is typically on the order of 10<sup>-11</sup> cm<sup>3</sup> molecule<sup>-1</sup> s<sup>-1</sup> with a negative temperature dependence (Atkinson et al., 2006). As for RO<sub>2</sub>+RO<sub>2</sub> reactions, the rate coefficients vary over a wide range from 10<sup>-17</sup> to 10<sup>-10</sup> cm<sup>3</sup> molecule<sup>-1</sup> s<sup>-1</sup> (Berndt et al., 2018a; Tomaz et al., 2021). The impact of temperature on RO<sub>2</sub> cross reactions was reported to be dependent on RO<sub>2</sub> structures, and there is no clear conclusion on the temperature influence on the rate coefficients and the product branching ratios of  
60 monoterpene-derived and sesquiterpene-derived RO<sub>2</sub> cross reactions as for now (Atkinson et al., 2006). [HO<sub>2</sub>]/[RO<sub>2</sub>] is not only critical in determining the fate of RO<sub>2</sub>, but also important for evaluating whether the laboratory results can be compared with realistic situations. Atmospheric [HO<sub>2</sub>]/[RO<sub>2</sub>] is usually larger than 1, and the modeled global surface [HO<sub>2</sub>]/[RO<sub>2</sub>] was reported as 2–9 in January and 0.75–2 in July (Peng et al., 2022). However, in simulation chamber or flow tube studies, without HO<sub>2</sub> sources, the [HO<sub>2</sub>]/[RO<sub>2</sub>] could be significantly lower than 1, leading to RO<sub>2</sub> radicals primarily undergoing self- or cross-  
65 reactions.

In the past few years, the generation of dimers has attracted increasing attention due to the low volatility of dimers, and is recognized as an important process in particle nucleation and growth (Donahue et al., 2012; Kristensen et al., 2013; Müller et al., 2008). Some particle-phase reactions, including hemiacetal reactions of peroxides and carbonyls, noncovalent clustering of carboxylic acids, and aldol condensation reactions, could contribute to dimers formation, however, these pathways were not  
70 able to adequately explain the dimers observed, and gas-phase reaction pathways were proposed to be important (DeVault and Ziemann, 2021; Hasan et al., 2021; Kenseth et al., 2018). The gas-phase formation mechanisms of dimers include reactions involving SCIs and RO<sub>2</sub> radicals, and clustering of carboxylic acids (Berndt et al., 2018a; Chen et al., 2019; Kristensen et al., 2014; Valiev et al., 2019). Some field studies investigated the formation of dimers and showed potential temperature effects (Claudia et al., 2017; Yasmeeen et al., 2010). The temperature dependence reported for dimers formation was contradictory due  
75 to the uncertainty of temperature impact on different formation pathways (Kristensen et al., 2020; Zhang et al., 2015). In this study, the performances of SCIs and RO<sub>2</sub> radicals in the generation of dimers and SOA were elaborately studied from 248 K to 298 K in β-pinene ozonolysis. Dimers' formation was particularly focused on, because of their importance in particle generation and growth, as well as their role of an essential indicator for RO<sub>2</sub> and SCIs reactions. Monoterpenes are critical precursors for the generation of reactive intermediates and aerosols in the atmosphere. The oxidation of α-pinene has been  
80 broadly investigated, however, different isomers of monoterpenes have different reaction mechanisms due to their different molecule structures. Here β-pinene, which has considerable SCIs yields during ozonolysis, was chosen as the research object



(Nguyen et al., 2009). As the second most abundant monoterpene,  $\beta$ -pinene with a global annual emission rate of 10–50 TgC contributes to about 20% of monoterpenes, and is regarded as a representative exocyclic monoterpene (Guenther et al, 2012; Sindelarova et al., 2014; Wiedinmyer et al, 2004).

## 85 2 Experimental

### 2.1 Experiments

The experiments were conducted in the AIDA (Aerosol Interaction and Dynamics in the Atmosphere) simulation chamber at the Karlsruhe Institute of Technology (KIT). The AIDA chamber is a cylindrical aluminum vessel of 84.5 m<sup>3</sup> in volume. It was operated as a continuously stirred reactor with a mixing time of 1–2 min achieved by a fan located 1 m above the bottom  
90 of the chamber. The temperature inside the chamber was controlled at 298±0.3 K, 273±0.3 K, and 248±0.3 K during this work.  $\beta$ -pinene (99%, Alfa Aesar) was evaporated and added to the chamber with a flow of synthetic air. The initial mixing ratio of  $\beta$ -pinene at 298 K was 19.3±1.2 ppb, and the initial molecule concentration of  $\beta$ -pinene in each experiment was controlled to be similar, resulting in correspondingly lower mixing ratios at lower temperatures as illustrated in Table 1. In the experiments investigating SCIs reactions, 90±10 ppb of formic acid (FA, ≥ 98%, Sigma-Aldrich) was evaporated and added before O<sub>3</sub>  
95 injection. FA was selected as a SCIs scavenger because of its high efficiency of consuming SCIs with a reaction coefficient of larger than 1×10<sup>-10</sup> cm<sup>3</sup> molecule<sup>-1</sup> s<sup>-1</sup> (Lin and Chao, 2017). O<sub>3</sub> was generated by a silent discharge generator (Semozon 030.2, Sorbios) in pure oxygen. O<sub>3</sub> concentrations were elevated as temperature decreased due to the positive temperature dependence of the  $\beta$ -pinene ozonolysis reaction, resulting in similar ozonolysis rates at different temperatures. CO (40% in nitrogen, Basi Schöberl GmbH) was added and used as an OH radical scavenger and a precursor for HO<sub>2</sub> radicals. Different CO  
100 concentrations were used to modify the [HO<sub>2</sub>]/[RO<sub>2</sub>], and in the following these conditions are denoted as low (L), middle (M), and high (H) [HO<sub>2</sub>]/[RO<sub>2</sub>] conditions.

Before each experiment, the AIDA chamber was evacuated to around 1 Pa, flushed several times with 10 hPa of synthetic air, and filled to 1 atm with dry or humidified synthetic air. About 1000 cm<sup>-3</sup> ammonium sulfate (AS) particles (mode diameter: 235–245 nm) were generated by an ultrasonic nebulizer (Sinaptec NA2000), dried, and introduced in each experiment as seed  
105 particles to reduce wall losses of the semi-volatile products. In most experiments, to avoid the impact of water vapor on the radical chemistry and the measurements, the water vapor mixing ratio was controlled to be 1–3 ppm. The relative humidity (RH) was increased in the experiments simulating the water vapor interference in the atmosphere. Table 1 shows a summary of the experimental conditions in this study.

### 2.2 Instrumentation

110 The concentrations of gas-phase  $\beta$ -pinene and low-oxidized products, such as carbonyls, were measured by a proton-transfer-reaction time-of-flight mass spectrometer (PTR-ToF-MS 4000, Ionicon Analytic GmbH). The data was analyzed by PTR viewer 3.3.12. The inlet flow was 30 standard cubic centimeter per minute (SCCM), and a bypass flow of 3.9 standard liter per minute (SLM) was added to reduce the residence time in the Silcosteel sampling tube. The PTR-MS was calibrated with a gas standard (Ionicon Analytic GmbH), and a transmission curve was determined to calculate the concentrations of compounds  
115 not present in the gas standard. The sensitivity of  $\beta$ -pinene was 69.7±3.6 cps ppb<sup>-1</sup> for 10<sup>6</sup> cps H<sub>3</sub>O<sup>+</sup>. The O<sub>3</sub> concentrations were measured by an O<sub>3</sub> monitor (O<sub>3</sub>-41M, Environment). CO concentrations were measured by a CO monitor (NGA 2000, Rosemount Analytic). Water vapor concentrations were measured by a frost point mirror hygrometer (373LX, MBW) and in situ by a tuneable diode laser at 1370 nm (Fahey et al., 2014).

Particle size distributions and number concentrations were measured by a scanning mobility particle sizer (SMPS) consisting  
120 of a differential mobility analyzer (DMA 3071, TSI Inc.) and a condensation particle counter (CPC 3772, TSL Inc.). The sampling flow was 0.3 SLM, and the sheath air flow was 3 SLM. The diameter range measured was 13.6–736.5 nm. A high-



resolution time-of-flight aerosol mass spectrometer (HR-ToF-AMS, Aerodyne Inc.) was used to measure the aerosol mass size distribution versus the vacuum aerodynamic diameter. The instrument was calibrated with ammonium nitrate particles. The PIKA v1.80C software was used to analyse the AMS data.

- 125 Gas-phase and particle-phase oxidized products were measured by the Filter Inlet for Gas and Aerosols (FIGAERO, Aerodyne Inc.) coupled to a high-resolution time-of-flight chemical ionization mass spectrometer (HR-ToF-CIMS, Aerodyne Inc.) employing  $\Gamma^-$  for ionisation. Gas-phase samples were collected from the chamber through a 1/4-inch FEP tube at 6 SLM, resulting in a sampling residence time of less than 1 s to reduce the loss in the tube. 2 SLM of the gas flow went to the CIMS and was analyzed online. Particle-phase compounds were collected on PTFE filters (2  $\mu\text{m}$ , SKC Inc.) through a 1/4-inch
- 130 stainless-steel tube at 6 SLM. After collection the filter samples were stored at 253 K. After the experiments these filters were heated by FIGAERO-CIMS using a flow of ultra-high-purity nitrogen as carrier gas following a thermal desorption procedure from 296 K to a maximum temperature of 473 K with a total desorption time of 35 min. Integration of the thermal desorption profiles, i.e., thermograms, of individual compounds yields their total particle-phase signals. The data were analyzed with the Tofware software v3.1.2, and the reagent ion  $\Gamma^-$  was subtracted from the mass-to-charge ratio of all the molecules shown below.
- 135 Background measurements for both the gas and particle phase were done before adding the reactants, and the background signals were subtracted from the results. All ion signals were normalized to  $10^6$  cps  $\Gamma^-$  for comparison, and particle-phase signals were also normalized to the sampling volume. Pinic acid ( $\text{C}_9\text{H}_{14}\text{O}_4$ ) was used to calibrate the CIMS, and a sensitivity of  $12.6 \pm 1.5$  cps ppt $^{-1}$  for  $10^6$  cps  $\Gamma^-$  was observed. Although this value could not represent the sensitivities of all compounds measured by CIMS, as the most abundant product formed during the reaction, the calibration of pinic acid could give some
- 140 helpful reference information. The typical instrumentation and the schematic of the AIDA chamber are shown in Fig. S1.

### 3 Modelling

#### 3.1 Chemical kinetic model

- Here we used a box model run by the IDL-based EASY package to simulate the chemical kinetics of the reaction system and to determine the  $[\text{HO}_2]/[\text{RO}_2]$  selected in the experiments. The  $\beta$ -pinene reaction mechanism was taken from the Master
- 145 Chemical Mechanism (MCM) v3.3.2 (<http://mcm.leeds.ac.uk/MCM>). When CO was used to adjust  $[\text{HO}_2]/[\text{RO}_2]$  by reacting with OH radicals, the possibility of CO reacting with SCIs also needed to be estimated. The reaction coefficients of SCIs with CO are usually reported as smaller than  $10^{-18}$  cm $^3$  molecule $^{-1}$  s $^{-1}$  (Eskola et al., 2018; Kumar et al., 2014, 2020; Vereecken et al., 2015), according to which this reaction was calculated in the model and was regarded as too slow to make a difference to SCIs reactions. Another concern of using different CO concentrations was how it would influence the OH reactions in the
- 150 system. The quantities of  $\beta$ -pinene consumption by reactions of OH and  $\text{O}_3$  were calculated, and the temperature did not significantly impact the oxidation pathways of  $\beta$ -pinene. At low  $[\text{HO}_2]/[\text{RO}_2]$ , the amount of  $\beta$ -pinene oxidized by OH radicals were only about 1% versus  $\text{O}_3$  at the end of the experiment, and this ratio increased to about 2.4% and 6%, respectively, at middle and high  $[\text{HO}_2]/[\text{RO}_2]$  conditions as shown in Fig. S2. The results indicate that even at high  $[\text{HO}_2]/[\text{RO}_2]$ , ozonolysis was still the dominant reaction pathway in the system and could account for more than 90% of  $\beta$ -pinene oxidation.
- 155 Figure 1 shows the modeled  $[\text{HO}_2]/[\text{RO}_2]$  evolutions for different experimental conditions. With higher  $\text{HO}_2$  concentration (Fig. S3),  $\text{RO}_2$  consumption by reacting with  $\text{HO}_2$  was accelerated, resulting in lower  $\text{RO}_2$  concentration and higher  $[\text{HO}_2]/[\text{RO}_2]$ . The average  $[\text{HO}_2]/[\text{RO}_2]$  before 7000 s of reaction time at low, middle, and high  $[\text{HO}_2]/[\text{RO}_2]$  conditions were calculated to be 0.34, 1.06, and 1.53 at 298 K; 0.33, 1.15, and 1.68 at 273 K; 0.30, 1.26, and 1.88 at 248 K, indicating that  $[\text{HO}_2]/[\text{RO}_2]$  was effectively adjusted during the reaction. In addition to the impact of CO concentration, temperature also has
- 160 influence on  $[\text{HO}_2]/[\text{RO}_2]$ . The higher  $[\text{HO}_2]/[\text{RO}_2]$  calculated for lower temperatures can be attributed to the negative temperature dependence of the  $\text{RO}_2+\text{HO}_2$  reactions, of which the rate coefficients at 248 K are typically more than twice of those at 298 K. The temperature dependence of  $\text{RO}_2+\text{RO}_2$  reactions was not considered in the box model due to the complexity





of this kind of reactions (Atkinson et al., 2006). If the majority of  $\text{RO}_2+\text{RO}_2$  reactions in  $\beta$ -pinene oxidation have negative temperature dependence, the  $\text{RO}_2$  concentrations at lower temperatures would be overestimated in the model due to the faster consumption of  $\text{RO}_2+\text{RO}_2$  reactions on  $\text{RO}_2$  radicals, and the  $[\text{HO}_2]/[\text{RO}_2]$  is underestimated. Conversely, if the majority of  $\text{RO}_2+\text{RO}_2$  reactions in  $\beta$ -pinene oxidation have positive temperature dependence, the  $\text{RO}_2$  concentrations at lower temperatures would be underestimated, and the  $[\text{HO}_2]/[\text{RO}_2]$  is supposed to be lower.

### 3.2 Aerosol dynamic model

The aerosol dynamic model COSIMA was used to simulate the dynamics of aerosols in the chamber (Naumann, 2003; Saathoff et al., 2009). For products formed from oxidation reactions, gas-particle partitioning and wall loss processes are calculated by this model. As for particles, the coagulation, condensation, evaporation, sedimentation deposition, and diffusion to the walls are calculated. Simulations started with a measured particle size distribution, and an example of the comparison between measured and modeled particle size distribution is shown in Fig. S4.

The AIDA walls can be considered as an irreversible sink especially for acidic gas-phase species and particles, which are important for determining SOA formation. Here the wall loss rates of different species were evaluated. For  $\beta$ -pinene, we observed the time variation of  $\beta$ -pinene before adding  $\text{O}_3$ , and found that the wall loss of  $\beta$ -pinene was negligible at all temperatures. Two abundant carbonyl products, nopinone and formaldehyde (HCHO), were measured, and their concentrations did not show obvious decrease in two hours, indicating that the wall loss for such kind of carbonyl compounds could also be ignored in the timescale of this study. As for  $\text{O}_3$ , it was observed that after almost all  $\beta$ -pinene was reacted, the concentration of  $\text{O}_3$  kept decreasing. Based on the decreasing tendency, the wall loss rate constants of  $\text{O}_3$  were estimated to be  $(9.0\pm 1.0) \times 10^{-6} \text{ s}^{-1}$  at 298 K,  $(5.0\pm 0.5) \times 10^{-6} \text{ s}^{-1}$  at 273 K, and  $(4.0\pm 0.5) \times 10^{-6} \text{ s}^{-1}$  at 248 K. For organic acids, the aluminum wall acts as a significant sink. Here we calculated the wall loss rates of FA and  $\text{C}_9\text{H}_{14}\text{O}_4$  (pinic acid and homoterpenylic acid). It was estimated that the wall loss rate constant of FA was  $(2.5\pm 0.5) \times 10^{-4} \text{ s}^{-1}$  at 298 K,  $(1.2\pm 0.7) \times 10^{-4} \text{ s}^{-1}$  at 273 K, and  $(1.1\pm 0.3) \times 10^{-4} \text{ s}^{-1}$  at 248 K. For  $\text{C}_9\text{H}_{14}\text{O}_4$ , the wall loss rate constants were  $(2.6\pm 0.5) \times 10^{-4} \text{ s}^{-1}$ ,  $(1.2\pm 0.4) \times 10^{-4} \text{ s}^{-1}$ , and  $(1.0\pm 0.4) \times 10^{-4} \text{ s}^{-1}$  at 298 K, 273 K, and 248 K, respectively, indicating that the wall loss rates of organic acids were higher at higher temperature. This is consistent with a limitation of their wall loss rates by diffusion through the laminar layer at the chamber wall. The mixing ratios of gas-phase  $\text{C}_9\text{H}_{14}\text{O}_4$  before and after wall loss correction are shown in Fig. S5 for different temperatures. These wall loss rates were used in the COSIMA model to simulate the impact of wall losses on SOA formation.

## 4 Results and discussion

The discussion started from the temperature dependence of SOA yield and composition in  $\beta$ -pinene ozonolysis. The impact of changing  $[\text{HO}_2]/[\text{RO}_2]$  and scavenging SCIs on dimers and SOA were then investigated at different temperatures. The temperature dependences of SCIs-controlled and  $\text{RO}_2$ -controlled dimers were compared. Furthermore, the temperature influence on the reaction mechanisms of SCIs and  $\text{RO}_2$  were discussed to explain dimer formation mechanisms at different temperatures.

### 4.1 Temperature dependence of SOA formation

With the reaction proceeding, the SOA mass concentration successively increased and reached stable values as a result of both the SOA formation and wall loss processes. Figure 2 shows the typical evolution of  $\beta$ -pinene,  $\text{O}_3$ , SOA mass concentrations and mass size distributions, and the line in Fig. 2A represents the SOA mass concentration simulated by the aerosol dynamic model after wall loss correction. In most cases, filter samples were collected after 7000 s, when more than 90% of  $\beta$ -pinene was consumed, ensuring that the quantities of  $\beta$ -pinene oxidized were similar at different experimental conditions. Although seed particles were added as condensational sink, new particle formation still occurred, which could be seen in Fig. 2B. The



effective density of SOA is determined by comparing the mass and volume size distribution measured by SMPS and AMS, respectively (DeCarlo et al., 2004). The density of SOA formed from  $\beta$ -pinene ozonolysis was calculated as  $1.28 \pm 0.09 \text{ g} \cdot \text{cm}^{-3}$ , which is in agreement with previously reported values (Bahreini et al., 2005; Kostenidou et al., 2007), and the effect of temperature on SOA density was found to be not significant.

The SOA yields ( $Y_{\text{SOA}}$ ) are calculated as ratio of the SOA mass concentration ( $\mu\text{g} \cdot \text{m}^{-3}$ ) versus the mass concentration of  $\beta$ -pinene reacted ( $\mu\text{g} \cdot \text{m}^{-3}$ ). The SOA yields determined for different experimental conditions are shown in Fig. 3. The SOA yield at 298 K and low  $[\text{HO}_2]/[\text{RO}_2]$  was  $(12.8 \pm 1.0) \%$ , which is in the range of previously reported SOA yield for  $\beta$ -pinene ozonolysis (Lee et al., 2006; Xu et al., 2021). When the temperature decreased to 273 K, the SOA yield increased to  $(15.5 \pm 1.1) \%$  at low  $[\text{HO}_2]/[\text{RO}_2]$  due to both the promoted gas to particle partitioning and less wall losses of semi-volatile products. However, with the temperature further decreasing to 248 K, the SOA formation was inhibited and the SOA yield decreased to  $(9.1 \pm 0.6) \%$ , which could not be explained by the partitioning processes and wall loss effects. The model calculations of the masses of particle lost and gases lost to the walls are shown in Fig. 3 for different temperatures. The results demonstrated that the particles lost to the walls accounted for less than 10% of the SOA mass concentrations at all temperatures within the timescale of the experiment, and the mass of gases lost to the walls was largest at 298 K of about 25.5% in total SOA mass. The impact of temperature on SOA formation in  $\beta$ -pinene ozonolysis was found to be not monotonic. Such a temperature dependence of SOA formation was also observed in  $\beta$ -pinene ozonolysis in von Hessberg et al. (2009) from 263 K to 303 K, indicating the impact of subzero temperatures on the rate coefficients or product branching ratios of some reactions, which contribute to the formation of SVOCs and LVOCs.

Increasing  $[\text{HO}_2]/[\text{RO}_2]$  leads to reduced SOA formation at all temperatures, indicating that in  $\beta$ -pinene ozonolysis,  $\text{RO}_2 + \text{RO}_2$  reactions contribute more to SVOCs and LVOCs formation compared to  $\text{RO}_2 + \text{HO}_2$  reactions. This impact of increasing  $[\text{HO}_2]/[\text{RO}_2]$  on SOA formation from alkenes with an exocyclic double bond observed in this study is consistent with previous studies (Docherty and Ziemann, 2003; Keywood et al., 2004). Compared to low  $[\text{HO}_2]/[\text{RO}_2]$  (0.30–0.34) condition, the SOA yield decreased by 25–35% for middle  $[\text{HO}_2]/[\text{RO}_2]$  (1.06–1.26) condition, and 45–70% for high  $[\text{HO}_2]/[\text{RO}_2]$  (1.53–1.88) condition. The suppression of increasing  $[\text{HO}_2]/[\text{RO}_2]$  on SOA formation was larger at lower temperatures. Scavenging SCIs inhibited SOA formation substantially at all temperatures, with decreasing SOA yields in the range of 50–70%. To avoid unwanted interferences from extremely high concentrations of FA on both aerosols and measurements, we added moderate concentrations of FA. Considering previously reported SCIs scavenging by organic acids in monoterpene ozonolysis and the reduction of the products observed, the concentration of FA used in this study was estimated to be sufficient for scavenging more than 70% of all SCIs (Gong and Chen, 2021). The results showed the importance of SCIs and  $\text{RO}_2$  in SOA formation from 248 K to 298 K, and their reaction mechanisms and products formation deserved further analysis.

#### 4.2 SOA composition and abundance of dimers

Monomers with molecule formulas of  $\text{C}_{8-10}\text{H}_{8-20}\text{O}_{3-10}$  and dimers with molecule formulas of  $\text{C}_{16-20}\text{H}_{22-40}\text{O}_{4-12}$  were identified by FIGAERO-CIMS in the particle phase. The normalized signals of all particulate  $\text{C}_x\text{H}_y\text{O}_z$  are shown in Fig. S6. Monomers and dimers usually account for 54–64% and 12–20% of total particle-phase signal intensities, and their mass defect plots at different temperatures are shown in Fig. S7. Fractions of different dimer species are shown in Fig. 4A. The  $\text{C}_{20}$  dimers had a lower abundance accounting for only  $\sim 5\%$  of all dimers, due to which the formation mechanisms of  $\text{C}_{20}$  dimers were not discussed in detail in the following. The fractions of  $\text{C}_{17}$ ,  $\text{C}_{18}$ , and  $\text{C}_{19}$  dimers were 30–40%, 20–40%, and 10–20% in total dimers. For  $\text{C}_{16}$  dimers, their fraction in dimers decreased from 25–40% at 298 K to  $\sim 10\%$  at 248 K. Since we could not calibrate the sensitivity of our CIMS for dimers, assuming a similar sensitivity as that of pinic acid, the contribution of dimers to the SOA mass was estimated to be 17%–21%.

The normalized signals of  $\text{C}_{16-19}$  dimers for different experimental conditions are shown in Fig. S8, demonstrating that both changing  $[\text{HO}_2]/[\text{RO}_2]$  and scavenging SCIs significantly impact the formation of  $\text{C}_{16-19}$  dimers by influencing their gas-phase



formation pathways. In addition to gas-phase reactions, the contribution of particle-phase reactions to dimers formation was  
245 evaluated. If reactions of closed-shell products in the particle phase could significantly contribute to dimers, the signal of  
dimers should have a quadratic relation with the signal of monomers in the particle phase. However, we found a linear  
correlation between the particle-phase dimers and monomers as shown in Fig. S9, and such a phenomenon was also reported  
in  $\alpha$ -pinene oxidation (Zhao et al., 2018), indicating that the contribution of particle-phase reactions to dimers was not dominant  
in this reaction system. It was also reported that the clustering of acids in the gas phase was a possible formation pathway for  
250 dimers (Claeys et al., 2009). Assuming the most abundant acids  $C_9H_{14}O_4$  could get clustered and generate  $C_{18}H_{28}O_8$  in the gas  
phase, it was calculated that the fraction of  $C_{18}H_{28}O_8$  in total dimers was only about 1%, suggesting that this pathway was not  
an efficient formation pathway for dimers.

Figure 4B shows the temperature dependence of the relative abundance of  $C_{16-19}$  dimers, indicating that differences exist in  
their formation mechanisms. For  $C_{16}$  dimers, their abundances at 298 K and 273 K were quite similar, while they decreased  
255 by more than 60% at 248 K, suggesting that the major formation pathway of  $C_{16}$  dimers was inhibited to a large extent. For  
 $C_{17-19}$  dimers, their formation showed increase of about 40% when temperature decreased from 298 K to 273 K, which could  
be partially attributed to the decrease of volatilities and less wall losses. Compared to  $C_{16}$  dimers, of which the particulate  
abundance did not show obvious increase with temperature decreasing from 298 K to 273 K, the variations of other dimers  
demonstrated that the inhibition of decreasing temperature on the formation of  $C_{16}$  dimers was so strong that it diminished the  
260 effects of decreasing volatilities and wall losses. When the temperature further decreased to 248 K,  $C_{17}$  dimers decreased by  
about 45%, and  $C_{18}$  and  $C_{19}$  dimers decreased by about 35%, indicating the influence of lower temperature on the formation  
pathways also happened to  $C_{17-19}$  dimers. One possible reason for the inhibition of dimers' formation at 248 K is the  
temperature impact on HOMs formation, since the autoxidation rate coefficients are prompted rapidly by increasing  
temperature (Praske et al., 2017). Ehn et al. (2014) reported that the formation of HOMs, which could also be regarded as  
265 extremely low-volatile organic compounds (ELVOCs), was about two orders of magnitude lower in  $\beta$ -pinene ozonolysis than  
in  $\alpha$ -pinene ozonolysis. In this study, the HOMs observed (monomers with 6–10 and dimers with 8–12 oxygen atoms) were a  
small part of the total particle-phase monomers and dimers' signal, indicating that the decreasing autoxidation rate at lower  
temperatures could not fully explain the suppression of dimers formation below 273 K. In the next section, we will discuss the  
contribution of other formation pathways to dimers.

270 It is noted that some monomers show two peaks in their thermograms. Figure S10 shows the thermograms of two abundant  
monomers formed during the reaction, i.e.,  $C_8H_{12}O_4$  (terpenylic acid) and  $C_9H_{14}O_4$  (pinic acid and homoterpenylic acid).  
Lopez-Hilfike et al. (2015) measured similar thermograms of  $C_8H_{12}O_4$  and  $C_9H_{14}O_4$  from aerosols generated in  $\alpha$ -pinene  
oxidation, and they claimed that according to their calibrated desorption-temperature relation, it was unlikely that such a big  
difference existed between the vapor pressures of isomers, suggesting that the thermal decomposition of some unstable  
275 oligomers, which probably contained noncovalent bonds, contributed to the second desorption peak. We estimated that the  
fraction of the second peak in the thermograms of  $C_8H_{12}O_4$  and  $C_9H_{14}O_4$  accounted for 30–50%. The thermograms of two  
abundant dimers  $C_{17}H_{26}O_8$  and  $C_{18}H_{28}O_6$  are shown in the figure for comparison. These two dimers showed one peak in their  
thermograms, in which the desorption temperatures corresponding to the peak signal ( $T_{max}$ ) were around 100 °C. Although a  
small fraction of the dimers showed double peaks in their thermograms, the fraction of the second peak in the total signal was  
280 usually less than 35%. Due to the thermal decomposition of some unstable dimers, the signal fraction of dimers in  $C_xH_yO_z$   
reported in this study represents a lower limit.

### 4.3 Chemistry of SCIs and their impact on dimers

The scavenging of SCIs leads to a reduce of more than 40% in total dimers from 248 K to 298 K, indicating the significant  
contribution of  $\beta$ -pinene-derived SCIs to dimers formation through bimolecular reactions. After the addition of  $O_3$  to  $\beta$ -pinene,  
285 the primary ozonide generates and usually has two decomposition pathways. One leads to an excited  $C_9$ -Criegee intermediate



and HCHO, and the other forms the excited  $\text{CH}_2\text{OO}$  and nopinone. In previous studies, the formation of excited  $\text{C}_9$ -Criegee intermediates was reported to be the primary pathway, which could account for 80–90% of the primary ozonide decomposition (Ma and Marston, 2008; Nguyen et al., 2009). Figure S11 shows the formation of HCHO and nopinone as a function of reacted  $\beta$ -pinene at 298 K for different  $[\text{HO}_2]/[\text{RO}_2]$ . Both the formation of HCHO and nopinone show good linear correlation with  $\beta$ -pinene reacted. Different  $[\text{HO}_2]/[\text{RO}_2]$  caused by different CO concentrations did not influence HCHO and nopinone formation, confirming that the CO reaction with SCIs was negligible. At the other two temperatures, similar correlations between HCHO and nopinone formation and  $\beta$ -pinene consumption were observed, indicating that temperature would not influence the early reaction steps of Criegee intermediates' generation. The molar yields of HCHO and nopinone are calculated as  $0.630 \pm 0.004$  and  $0.160 \pm 0.003$ , which are in the range of values reported previously (Elayan et al., 2019; Lee et al., 2006; Winterhalter et al., 2000). Considering the yields of HCHO and nopinone observed in this study and the values suggested in previous studies, the branching ratios of the formation of the excited  $\text{C}_9$ -Criegee intermediate and the excited  $\text{CH}_2\text{OO}$  from ozonide decomposition were modified from 0.6 and 0.4 to 0.8 and 0.2 in the MCM mechanism. It was reported that the yield of  $\text{C}_9$ -SCIs was about 0.35 in  $\beta$ -pinene ozonolysis, and the yield of stabilized  $\text{CH}_2\text{OO}$  was about 0.1 (Ahrens et al., 2014; Winterhalter et al., 2000; Zhang and Zhang, 2005). Based on this the branching ratios of forming stabilized  $\text{C}_9$  and  $\text{C}_1$  Criegee intermediates from excited Criegee intermediates (ECIs) were adjusted to be 0.4 and 0.5. Another important reaction pathway of ECIs is isomerization and decomposition, forming OH radicals. The OH yield from  $\beta$ -pinene ozonolysis was reported to be about 0.3, which is half of that from  $\alpha$ -pinene ozonolysis (Atkinson et al., 1992; Nguyen et al., 2009). Table S1 shows the summary of the main updates to the formation of  $\beta$ -pinene-derived Criegee intermediates in the MCM mechanism.

Scavenging of SCIs led to a significant suppression of dimers and SOA formation for different  $[\text{HO}_2]/[\text{RO}_2]$  conditions as shown by Fig. 5. The addition of SCIs scavenger was reported to lead to a decrease of  $\text{RO}_2$  concentrations in the range of 11–17%, which was critical for the results (Berndt et al., 2018b). At all temperatures, more than 50% of SOA formation was inhibited by scavenging SCIs, while dimers showed different temperature dependences. For  $\text{C}_{18}$  and  $\text{C}_{19}$  dimers, their decreases by scavenging SCIs were more than 50% at all temperatures, indicating that SCIs reactions are always a dominant source for  $\text{C}_{18}$  and  $\text{C}_{19}$  dimers. For  $\text{C}_{16}$  and  $\text{C}_{17}$  dimers, and especially for  $\text{C}_{16}$  dimers, the impact of scavenging SCIs varied with temperatures. At 298 K, the scavenging of SCIs showed a limited impact on  $\text{C}_{16}$  dimers' generation with about 20% decrease. With the temperature decreasing, the relative contribution of SCIs reactions for  $\text{C}_{16}$  dimers formation became larger. Considering the inhibited formation of  $\text{C}_{16}$  dimers at lower temperatures, it was attributed that the main formation pathway of  $\text{C}_{16}$  dimers was largely limited at low temperatures, resulting in an increase of the relative importance of SCIs reactions in  $\text{C}_{16}$  dimers formation.

To further investigate the dimers formation mechanism through SCIs reaction channel at different temperatures, the contribution of SCIs to individual dimers was paid attention to. The most abundant dimers  $\text{C}_{16-19}\text{H}_{22-32}\text{O}_5-9$  ( $\text{C}_{16}\text{H}_{22-28}\text{O}_6-9$ ,  $\text{C}_{17}\text{H}_{22-30}\text{O}_5-9$ ,  $\text{C}_{18}\text{H}_{24-30}\text{O}_4-8$ ,  $\text{C}_{19}\text{H}_{26-32}\text{O}_5-8$ ), which accounted for more than 70% of total dimer signals, were selected for further analysis of their formation mechanisms. For this purpose, we defined that if one dimer was suppressed by  $\geq 50\%$  when scavenging SCIs at all temperatures, it was classified as a SCIs-controlled dimer. For these abundant dimers, most of  $\text{C}_{18}$  and  $\text{C}_{19}$  dimers and half of  $\text{C}_{17}$  dimers are SCIs-controlled, while none of the  $\text{C}_{16}$  dimers are mainly contributed by SCIs reactions.  $\text{C}_9$ -SCIs contributed to  $\text{C}_{17-19}$  dimers through reacting with  $\text{C}_{8-10}$  products, which were more abundant in the gas phase compared to  $\text{C}_7$  products. Figure 6 shows the relative changes of SCIs-controlled and non-SCIs-controlled abundant dimers at 298 K or 248 K versus 273 K. For the dimers mainly controlled by SCIs reactions, more than half of them showed higher abundances at 248 K than at 298 K, suggesting that the contribution of SCIs reactions to these dimers was not suppressed, even though the gas-phase oxidized monomers' concentrations were lowest at 248 K. For non-SCIs-controlled dimers, they usually had much higher formation at 298 K than 248 K. The results demonstrate the importance of SCIs in contributing to dimers and SOA formation at lower temperatures. When considering the SOA formation potential of SCIs in the atmosphere, one limiting factor is the water vapor concentration. Although the reaction coefficient between SCIs and  $\text{H}_2\text{O}$  is not fast, and



330 this reaction depends on the structure of SCIs, it is still one of the most important sinks for SCIs due to the high concentrations  
of water vapor in the atmosphere (Lin and Chao, 2017). Through raising RH to 15% at 298 K ( $\text{H}_2\text{O}$ :  $1.15 \times 10^{17}$  molecule  $\text{cm}^{-3}$ )  
and 80% at 273 K ( $\text{H}_2\text{O}$ :  $1.29 \times 10^{17}$  molecule  $\text{cm}^{-3}$ ), about 40% of inhibition on dimers' formation was observed. When  
increasing RH to 70% at 248 K ( $\text{H}_2\text{O}$ :  $1.73 \times 10^{16}$  molecule  $\text{cm}^{-3}$ ), there was no obvious suppression on dimers, suggesting that  
the contribution of  $\beta$ -pinene to atmospheric SCIs and dimers could be more important in colder regions due to the less water  
vapor effects. The water vapor concentration could also influence the peroxy radical chemistry, while here this issue was not  
335 analyzed in detail.

#### 4.4 Specific $[\text{HO}_2]/[\text{RO}_2]$ impact at lower temperatures

The changing  $[\text{HO}_2]/[\text{RO}_2]$  showed significant impact on dimers formation, especially for lower temperatures, suggesting the  
influence of lower temperatures on  $\text{RO}_2$  reactions. The relative changes of particulate dimers and SOA with increasing  
 $[\text{HO}_2]/[\text{RO}_2]$  are shown in Fig. 7, which illustrates that the formation of dimers becomes more sensitive to  $[\text{HO}_2]/[\text{RO}_2]$  changes  
340 at lower temperatures. At 298 K, the decrease of dimers was within 10% from middle  $[\text{HO}_2]/[\text{RO}_2]$  to high  $[\text{HO}_2]/[\text{RO}_2]$ , and  
this value increased to about 20 % and 30% at 273 K and 248 K, respectively. At high  $[\text{HO}_2]/[\text{RO}_2]$ , the dimers abundances  
were about 69%, 56%, and 30% of those at low  $[\text{HO}_2]/[\text{RO}_2]$  at 298 K, 273 K, and 248 K, respectively.  $[\text{HO}_2]/[\text{RO}_2]$  impacted  
the dimers formation from  $\text{RO}_2+\text{RO}_2$  reactions as follows:

$$[\text{ROOR}] = \gamma \cdot [\text{RO}_2]^2 \quad (1)$$

345 Where  $[\text{RO}_2]$  is the concentration of  $\text{RO}_2$  in the gas phase;  $[\text{ROOR}]$  is the concentration of dimers formed;  $\gamma$  is the branching  
ratio of dimers formation from  $\text{RO}_2$  cross reactions. The  $\text{RO}_2$  concentrations were simulated in the box model for different  
conditions and are shown in Fig. S12. If  $\text{RO}_2$  radicals influence dimers formation predominately through  $\text{RO}_2+\text{RO}_2$  reactions,  
the dimer signal should have a linear correlation with  $[\text{RO}_2]^2$ . Figure 8 shows the correlations between dimers and  $[\text{RO}_2]^2$   
at different temperatures, demonstrating that  $\text{RO}_2$  cross reactions could explain the dimers variation at 298 K, while at 273 K and  
350 248 K, the correlation between dimers and  $[\text{RO}_2]^2$  is low. Although some uncertainties existed in the simulated  $\text{RO}_2$   
concentrations due to the lack of temperature dependence data for  $\text{RO}_2+\text{RO}_2$  reactions, from the comparison between different  
temperatures it could still be concluded that the variation of  $\text{RO}_2$  concentrations at low temperatures impacts other dimers  
formation pathways besides  $\text{RO}_2$  cross reactions.

For individual dimers, we defined that if one dimer was suppressed for  $\geq 20\%$  at middle  $[\text{HO}_2]/[\text{RO}_2]$  and  $\geq 40\%$  at high  
355  $[\text{HO}_2]/[\text{RO}_2]$ , it was classified as a  $\text{RO}_2$ -controlled dimer. The temperature dependences of  $\text{RO}_2$ -controlled dimers are shown  
in Fig. S13. The  $\text{RO}_2$ -controlled dimers included most of  $\text{C}_{16}$  and  $\text{C}_{19}$  dimers, and part of  $\text{C}_{17}$  and  $\text{C}_{18}$  dimers. For the dimers  
mainly controlled by  $\text{RO}_2$  reactions, in which  $\text{C}_{16}$  dimers accounted for more than 50%, they usually showed no obvious  
reduction at 298 K compared to 273 K, while they were significantly inhibited at 248 K, suggesting that the contribution of  
 $\text{RO}_2+\text{RO}_2$  reactions decreased at 248 K due to the decreasing rate coefficient or decreasing branching ratios of forming dimers.  
360 For the dimers controlled by both SCIs and  $\text{RO}_2$  reactions, their temperature dependences varied, which was hypothesized to  
be due to the combined effect of these two reaction pathways.

It is intriguing to find that at low temperatures, the variation of  $[\text{HO}_2]/[\text{RO}_2]$  has such a big influence on  $\text{C}_{18}$  dimers, which are  
significantly contributed by SCIs reactions. The particular impact of  $[\text{HO}_2]/[\text{RO}_2]$  at low temperatures on  $\text{C}_{18}$  dimers could be  
clearly represented by the formation of  $\text{C}_{18}\text{H}_{28}\text{O}_6$ , one of the most abundant dimers mainly generated from  $\text{C}_9$ -SCIs reaction  
365 with  $\text{C}_9\text{H}_{14}\text{O}_4$ . The gas-phase concentration of  $\text{C}_{18}\text{H}_{28}\text{O}_6$  decreases substantially if scavenging SCIs as Fig. 9, confirming that  
SCIs reactions are the dominant source for  $\text{C}_{18}\text{H}_{28}\text{O}_6$ . Figure 9A shows the total abundance of  $\text{C}_{18}\text{H}_{28}\text{O}_6$  in the gas and particle  
phase, and more than 90% of them stayed in the particle phase. At 298 K the formation of  $\text{C}_{18}\text{H}_{28}\text{O}_6$  was not sensitive to  
changing  $[\text{HO}_2]/[\text{RO}_2]$ , while with temperature decreasing to 273 K and 248 K, the  $[\text{HO}_2]/[\text{RO}_2]$  had an enlarging impact. We  
evaluated the influence of  $\text{C}_9$ -SCIs reactions with CO at lower temperatures. The formation of nopinone, as the main product  
370 from SCIs reaction with CO, is not notably influenced by CO concentration at all temperatures, confirming that the CO



consumption on C<sub>9</sub>-SCIs is negligible. The [HO<sub>2</sub>]/[RO<sub>2</sub>] impact on gas-phase C<sub>9</sub>H<sub>14</sub>O<sub>4</sub> concentration was also considered since C<sub>9</sub>H<sub>14</sub>O<sub>4</sub> is the precursor for C<sub>18</sub>H<sub>28</sub>O<sub>6</sub> generation from C<sub>9</sub>-SCIs reactions. Figure S14 shows the gas-phase C<sub>9</sub>H<sub>14</sub>O<sub>4</sub> concentrations after wall loss correction at different temperatures, demonstrating the limited effect of [HO<sub>2</sub>]/[RO<sub>2</sub>] on C<sub>9</sub>H<sub>14</sub>O<sub>4</sub> formation. After excluding these two possible reasons, there is still the option that the [HO<sub>2</sub>]/[RO<sub>2</sub>] directly impacts SCIs reactions with RO<sub>2</sub> radicals, which contributes to dimers formation (Chhantyal-Pun et al., 2020b; Sakamoto et al., 2017). The potential contribution of C<sub>9</sub>-SCIs reaction with RO<sub>2</sub> radicals to dimers formation was evaluated using a box model, and conditions at 298 K and 248 K were chosen for comparison. Since the interference of water vapor was avoided, the unimolecular reaction of SCIs, including isomerization and decomposition, was the largest sink of SCIs in the reaction system compared with other bimolecular reactions and was crucial for determining the lifetime and concentration of SCIs (Cox et al., 2020). The rate coefficients of SCIs unimolecular reactions are strongly influenced by temperature. It was reported that the unimolecular reaction coefficient of (CH<sub>3</sub>)<sub>2</sub>COO-SCIs increased by a factor of four with temperature increasing by 40 K (Smith et al., 2016). As for CH<sub>3</sub>CHOO-SCIs, the unimolecular reaction coefficient increased by a factor of five with temperature increasing by 35 K (Robinson et al., 2022). Berndt et al. (2014) reported that the ratio of the (CH<sub>3</sub>)<sub>2</sub>COO-SCIs unimolecular reaction coefficient versus the reaction coefficient with SO<sub>2</sub> increased by a factor of 34 from 278 K to 343 K. Although some studies reported the unimolecular reaction coefficients of those simple SCIs, less is known about the unimolecular reactions of monoterpene-derived SCIs. Gong et al. (2021) estimated the unimolecular reaction coefficient of limonene-derived SCIs as 30 s<sup>-1</sup> and 100 s<sup>-1</sup> for different SCIs isomers at 298 K. In this study the unimolecular reaction coefficient of β-pinene-derived C<sub>9</sub>-SCIs was set as 75 s<sup>-1</sup> at 298 K, and 15 s<sup>-1</sup> at 248 K in box model. Chhantyal-Pun et al. (2020b) claimed that the reaction coefficient of CH<sub>2</sub>OO with RO<sub>2</sub> was (2.4±1.2) × 10<sup>-11</sup> cm<sup>3</sup> molecule<sup>-1</sup> s<sup>-1</sup>. Zhao et al. (2017) reported a negative temperature dependence of substituted alkyl peroxy radicals' reaction with Criegee intermediates, of which the reaction coefficient would increase one order of magnitude for temperature decreasing from 400 K to 250 K. Based on the reported values, the reaction coefficient of SCIs and RO<sub>2</sub> was set as 2 × 10<sup>-11</sup> cm<sup>3</sup> molecule<sup>-1</sup> s<sup>-1</sup> at 298 K, and 8 × 10<sup>-11</sup> cm<sup>3</sup> molecule<sup>-1</sup> s<sup>-1</sup> at 248 K. The radicals formed from SCIs reaction with RO<sub>2</sub> further react with HO<sub>2</sub> and RO<sub>2</sub>, generating closed-shell dimers. The model results of dimers formation from C<sub>9</sub>-SCIs reaction with RO<sub>2</sub> are shown in Fig. 10. The modeled dimers formed from C<sub>9</sub>-SCIs reaction with RO<sub>2</sub> could account for less than 5% in total measured dimers at 298 K, and this value increased to more than 60% at 248 K, indicating a greater contribution of this reaction channel to dimers formation at 248 K. Compared to low [HO<sub>2</sub>]/[RO<sub>2</sub>] condition, the modeled dimers formed from C<sub>9</sub>-SCIs reaction with RO<sub>2</sub> decreased by 44% and 61% at middle and high [HO<sub>2</sub>]/[RO<sub>2</sub>] conditions, which helped to explain the observed [HO<sub>2</sub>]/[RO<sub>2</sub>] influence on dimers at lower temperatures. The higher stability of SCIs at lower temperatures also promoted the bimolecular reactions of SCIs with other closed-shell products, however, due to the decrease of gas-phase concentrations of those closed-shell products, and the potential temperature effect on dimers formation from these reactions, in this study the contribution of this reaction channel seemed to be more important at 298 K than 248 K. It is claimed that the temperature impacts on the rate coefficients and product branching ratios of monoterpene-derived SCIs reactions are still not well defined and need further study.

## 5 Conclusions

This study reveals the role of RO<sub>2</sub> radicals and SCIs in the formation of dimers and SOA in β-pinene ozonolysis at different temperatures, especially for colder conditions. Both of the reactive intermediates showed their significant influence on SOA yield and composition. Temperature not only impacts the compounds' volatilities, but also impacts the reaction mechanisms and products formation of RO<sub>2</sub> and SCIs reactions. The SOA yield is not monotonic with decreasing temperature in β-pinene ozonolysis due to the joint influence of positive- and negative-temperature-dependent processes. Such influence with varying temperatures could also exist in other VOCs oxidation systems, and help to explain the controversy on the temperature dependence of SOA yield and composition. The SOA formation potential of β-pinene is influenced by several parameters in





the atmosphere, such as temperature, RH, and  $[HO_2]/[RO_2]$ , which are to a large extent correlated to the chemistry of Criegee intermediates and peroxy radicals, suggesting that a constant yield is not sufficient to represent the SOA formation potential of  $\beta$ -pinene in models. The results provide evidence for the importance of SCIs in dimers and SOA formation at subzero  
415 temperatures, and the reactions of SCIs and  $RO_2$  with negative temperature dependence show increasing importance with decreasing temperature. These results can be used to improve the chemical mechanism modelling of monoterpenes and also SOA parameterization in transport models. The lifetime of SCIs becomes longer in colder regions due to lower temperatures and lower water vapor concentrations, while these intermediates still maintain high reactivities, suggesting the chemistry of SCIs plays an important role and requires more attention in winter and at higher altitudes.  
420

**Data availability.** The data are available via the repository KITopen (link to be added). Data are also available upon request to the corresponding author.  
425

**Supplement.** The supplement related to this article is available online.

**Author contributions.** YG and HS designed the study and carried out the experiments. FJ helped operate the instruments. YL operated PTR-MS and analyzed its data. YG analyzed the data, ran the models, and formatted the manuscript. All co-authors  
430 commented on the manuscript.

**Competing interests.** At least one of the co-authors is a member of the editorial board of Atmospheric Chemistry and Physics. The authors have no other competing interests to declare.

**Acknowledgments.** Technical support by the AIDA staff at IMK-AAF is gratefully acknowledged. YG is grateful to the Helmholtz-OCPC Fellowship Program.  
435

## References

- 440 Ahrens, J., Carlsson, P. T. M., Hertl, N., Olzmann, M., Pfeifle, M., Wolf, J. L., and Zeuch, T.: Infrared Detection of Criegee Intermediates Formed during the Ozonolysis of  $\beta$ -Pinene and Their Reactivity towards Sulfur Dioxide, *Angew. Chem. Int. Ed.*, 53, 715–719, doi: 10.1002/anie.201307327, 2014.
- Atkinson, R., Aschmann, S. M., Arey, J., and Shorees, B.: Formation of OH radicals in the gas phase reactions of  $O_3$  with a series of terpenes, *J. Geophys. Res.*, 97, 6065–6073, doi: 10.1029/92JD00062, 1992.
- 445 Atkinson, R., Baulch, D. L., Cox, R. A., Crowley, J. N., Hampson, R. F., Hynes, R. G., Jenkin, M. E., Rossi, M. J., Troe, J., and IUPAC Subcommittee: Evaluated kinetic and photochemical data for atmospheric chemistry: Volume II – gas phase reactions of organic species, *Atmos. Chem. Phys.*, 6, 3625–4055, doi: acp-6-3625-2006, 2006.
- Bahreini, R., Keywood, M. D., Ng, N. L., Varutbangkul, V., Gao, S., Flagan, R. C., Seinfeld, J. H., Worsnop, D. R., and Jimenez, J. L.: Measurements of secondary organic aerosol from oxidation of cycloalkenes, terpenes, and m-xylene using an aerodyne aerosol mass spectrometer, *Enviro. Sci. Technol.*, 39, 5674–5688, doi: 10.1021/es048061a, 2005.
- 450 Berndt, T., Jokinen, T., Sipilä, M., Mauldin III, R. L., Herrmann, H., Stratmann, F., Junninen, H., and Kulmala, M.:  $H_2SO_4$  formation from the gas-phase reaction of stabilized Criegee Intermediates with  $SO_2$ : Influence of water vapour content and temperature, *Atmos. Environ.*, 89, 603–612, doi: 10.1016/j.atmosenv.2014.02.062, 2014.



- Berndt, T., Scholz, W., Mentler, B., Fischer, L., Herrmann, H., Kulmala, M., and Hansel, A.: Accretion product formation  
455 from self- and cross-reactions of RO<sub>2</sub> radicals in the atmosphere, *Angew. Chem., Int. Ed.*, *57*, 3820–3824, doi:  
10.1002/anie.201710989, 2018a.
- Berndt, T., Mentler, B., Scholz, W., Fischer, L., Herrmann, H., Kulmala, M., and Hansel, A.: Accretion Product Formation  
from Ozonolysis and OH Radical Reaction of  $\alpha$ -Pinene: Mechanistic Insight and the Influence of Isoprene and Ethylene,  
*Environ. Sci. Technol.*, *52*, 11069–11077, doi: 10.1021/acs.est.8b02210, 2018b.
- 460 Chen, L., Huang, Y., Xue, Y., Shen, Z., Cao, J., and Wang, W.: Mechanistic and kinetics investigations of oligomer formation  
from Criegee intermediate reactions with hydroxyalkyl hydroperoxides, *Atmos. Chem. Phys.*, *19*, 4075–4091, doi:  
10.5194/acp-19-4075-2019, 2019.
- Chhantyal-Pun, R., McGillen, M. R., Beames, J. M., Khan, M. A. H., Percival, C. J., Shallcross, D. E., and Orr-Ewing, A. J.:  
Temperature-Dependence of the Rates of Reaction of Trifluoroacetic Acid with Criegee Intermediates, *Angew. Chem. Int. Ed.*,  
465 *56*, 9044–9047, doi:10.1002/anie.201703700, 2017.
- Chhantyal-Pun, R., Khan, M. A. H., Taatjes, C. A., Percival, C. J., Orr-Ewing, A. J., and Shallcross, D. E.: Criegee  
intermediates: production, detection and reactivity, *International Reviews in Physical Chemistry*, *39*, 385–424, doi:  
10.1080/0144235X.2020.1792104, 2020a.
- Chhantyal-Pun, R., Khan, M. A. H., Zachhuber, N., Percival, C. J., Shallcross, D. E., and Orr-Ewing, A. J.: Impact of Criegee  
470 Intermediate Reactions with Peroxy Radicals on Tropospheric Organic Aerosol, *ACS Earth Space Chem.*, *4*, 1743–1755, doi:  
10.1021/acsearthspacechem.0c00147, 2020b.
- Claeys, M., Iinuma, Y., Szmigielski, R., Surratt, J. D., Blockhuys, F., Van Alsenoy, C., Böge, O., Sierau, B., Gómez-González,  
Y., Vermeylen, R., Van der Veken, P., Shahgholi, M., Chan, A. W. H., Herrmann, H., Seinfeld, J. H., and Maenhaut, W.:  
Terpenylic Acid and Related Compounds from the Oxidation of  $\alpha$ -Pinene: Implications for New Particle Formation and  
475 Growth above Forests, *Environ. Sci. Technol.*, *43*, 6976–6982, doi: 10.1021/es9007596, 2009.
- Cox, R. A., Ammann, M., Crowley, J. N., Herrmann, H., Jenkin, M. E., McNeill, V. F., Mellouki, A., Troe, J., and Wallington,  
T. J.: Evaluated kinetic and photochemical data for atmospheric chemistry: Volume VII – Criegee intermediates, *Atmos. Chem.  
Phys.*, *20*, 13497–13519, doi: 10.5194/acp-20-13497-2020, 2020.
- DeCarlo, P. F., Slowik, J. G., Worsnop, D. R., Davidovits, P., and Jimenez, J. L.: Particle Morphology and Density  
480 Characterization by Combined Mobility and Aerodynamic Diameter Measurements. Part 1: Theory, *Aerosol Sci. Tech.*, *38*,  
1185–1205, doi: 10.1080/027868290903907, 2004.
- DeVault, M. P. and Ziemann, P. J.: Gas- and Particle-Phase Products and Their Mechanisms of Formation from the Reaction  
of  $\Delta$ -3-Carene with NO<sub>3</sub> Radicals, *J. Phys. Chem. A*, *125*, 10207–10222, 2021.
- Docherty, K. S. and Ziemann, P. J.: Effects of Stabilized Criegee Intermediate and OH Radical Scavengers on Aerosol  
485 Formation from Reactions of  $\beta$ -Pinene with O<sub>3</sub>, *Aerosol Sci. Technol.*, *37*, 877–891, doi: 10.1080/02786820300930, 2003.
- Donahue, N. M., Kroll, J. H., Pandis, S. N., and Robinson, A. L.: A two-dimensional volatility basis set – Part 2: Diagnostics  
of organic-aerosol evolution, *Atmos. Chem. Phys.*, *12*, 615–634, doi: 10.5194/acp-12-615-2012, 2012.
- Ehn, M., Thornton, J. A., Kleist, E., Sipilä, M., Junninen, H., Pullinen, I., Springer, M., Rubach, F., Tillmann, R., Lee, B.,  
Lopez-Hilfiker, F., Andres, S., Acir, I.-H., Rissanen, M., Jokinen, T., Schobesberger, S., Kangasluoma, J., Kontkanen, J.,  
490 Nieminen, T., Kurtén, T., Nielsen, L. B., Jørgensen, S., Kjaergaard, H. G., Canagaratna, M., Dal Maso, M., Berndt, T., Petäjä,  
T., Wahner, A., Kerminen, V.-M., Kulmala, M., Worsnop, D. R., Wildt, J., and Mentel, T. F.: A large source of low-volatility  
secondary organic aerosol, *Nature*, *506*, 476–479, doi: 10.1038/nature13032, 2014.
- Elayan, I. A., Almatarneh, M. H., and Hollett, J. W.: Reactivity of the anti-Criegee intermediate of  $\beta$ -pinene with prevalent  
atmospheric species, *Struct. Chem.*, *30*, 1353–1364, doi: 10.1007/s11224-019-1288-4, 2019.
- 495 Eskola, A. J., Döntgen, M., Rotavera, B., Caravan, R. L., Welz, O., Savee, J. D., Osborn, D. L., Shallcross, D. E., Percival, C.  
J., and Taatjes, C. A., Direct kinetics study of CH<sub>2</sub>OO + methyl vinyl ketone and CH<sub>2</sub>OO + methacrolein reactions and an



- upper limit determination for  $\text{CH}_2\text{OO} + \text{CO}$  reaction, *Phys. Chem. Chem. Phys.*, 20, 19373–19381, doi: 10.1039/c8cp03606c, 2018.
- Fahey, D. W., Gao, R.-S., Möhler, O., Saathoff, H., Schiller, C., Ebert, V., Krämer, M., Peter, T., Amarouche, N., Avallone, L. M., Bauer, R., Bozóki, Z., Christensen, L. E., Davis, S. M., Durr, G., Dyrhoff, C., Herman, R. L., Hunsmann, S., Khaykin, S. M., Mackrodt, P., Meyer, J., Smith, J. B., Spelten, N., Troy, R. F., Vömel, H., Wagner, S., and Wienhold, F. G.: The AquaVIT-1 intercomparison of atmospheric water vapor measurement techniques, *Atmos. Meas. Tech.*, 7, 3177–3213, doi: 10.5194/amt-7-3177-2014, 2014.
- Gong, Y. and Chen, Z.: Quantification of the role of stabilized Criegee intermediates in the formation of aerosols in limonene ozonolysis, *Atmos. Chem. Phys.*, 21, 813–829, doi: 10.5194/acp-21-813-2021, 2021.
- Greenberg, J. P., Guenther, A. B., Pétron, G., Wiedinmyer, C., Vega, O., Gatti, L.V., Tota, J., and Fisch, G.: Biogenic VOC emissions from forested Amazonian landscapes, *Global Change Biology*, 10, 651–662. doi: 10.1111/j.1365-2486.2004.00758.x, 2004.
- Guenther, A. B., Jiang, X., Heald, C. L., Sakulyanontvittaya, T., Duhl, T., Emmons, L. K., and Wang, X.: The Model of Emissions of Gases and Aerosols from Nature version 2.1 (MEGAN2.1): an extended and updated framework for modeling biogenic emissions, *Geosci. Model Dev.*, 5, 1471–1492, doi: 10.5194/gmd-5-1471-2012, 2012.
- Hallquist, M., Wenger, J. C., Baltensperger, U., Rudich, Y., Simpson, D., Claeys, M., Dommen, J., Donahue, N. M., George, C., Goldstein, A. H., Hamilton, J. F., Herrmann, H., Hoffmann, T., Iinuma, Y., Jang, M., Jenkin, M. E., Jimenez, J. L., Kiendler-Scharr, A., Maenhaut, W., McFiggans, G., Mentel, Th. F., Monod, A., Prévôt, A. S. H., Seinfeld, J. H., Surratt, J. D., Szmigielski, R., and Wildt, J.: The formation, properties and impact of secondary organic aerosol: current and emerging issues, *Atmos. Chem. Phys.*, 9, 5155–5236, doi: 10.5194/acp-9-5155-2009, 2009.
- Hasan, G., Valiev, R. R., Salo, V.-T., and Kurtén, T.: Computational Investigation of the Formation of Peroxide (ROOR) Accretion Products in the OH- and  $\text{NO}_3$ -Initiated Oxidation of  $\alpha$ -Pinene, *J. Phys. Chem. A*, 125, 10632–10639, doi: 10.1021/acs.jpca.1c08969, 2021.
- Jonsson, Å. M., Hallquist, M., and Ljungström, E.: The effect of temperature and water on secondary organic aerosol formation from ozonolysis of limonene,  $\Delta^3$ -carene and  $\alpha$ -pinene, *Atmos. Chem. Phys.*, 8, 6541–6549, doi: 10.5194/acp-8-6541-2008, 2008.
- Kanakidou, M., Seinfeld, J. H., Pandis, S. N., Barnes, I., Dentener, F. J., Facchini, M. C., Van Dingenen, R., Ervens, B., Nenes, A., Nielsen, C. J., Swietlicki, E., Putaud, J. P., Balkanski, Y., Fuzzi, S., Horth, J., Moortgat, G. K., Winterhalter, R., Myhre, C. E. L., Tsigaridis, K., Vignati, E., Stephanou, E. G., and Wilson, J.: Organic aerosol and global climate modelling: a review, *Atmos. Chem. Phys.*, 5, 1053–1123, doi: 10.5194/acp-5-1053-2005, 2005.
- Kenseth, C. M., Huang, Y. L., Zhao, R., Dalleska, N. F., Hethcox, J. C., Stoltz, B. M., and Seinfeld, J. H.: Synergistic  $\text{O}_3$ +OH oxidation pathway to extremely low-volatility dimers revealed in  $\beta$ -pinene secondary organic aerosol, *P. Natl. Acad. Sci.*, 115, 8301–8306, doi: 10.1073/pnas.1804671115, 2018.
- Keywood, M. D., Kroll, J. H., Varutbangkul, V., Bahreini, R., Flagan, R. C., and Seinfeld, J. H.: Secondary Organic Aerosol Formation from Cyclohexene Ozonolysis: Effect of OH Scavenger and the Role of Radical Chemistry, *Environ. Sci. Technol.*, 38, 3343–3350, doi: 10.1021/es049725j, 2004.
- Kostenidou, E., Pathak, R. K., and Pandis, S. N.: An Algorithm for the Calculation of Secondary Organic Aerosol Density Combining AMS and SMPS Data, *Aerosol Sci. Tech.*, 41, 1002–1010, doi: 10.1080/02786820701666270, 2007.
- Kristensen, K., Enggrob, K. L., King, S. M., Worton, D. R., Platt, S. M., Mortensen, R., Rosenoern, T., Surratt, J. D., Bilde, M., Goldstein, A. H., and Glasius, M.: Formation and occurrence of dimer esters of pinene oxidation products in atmospheric aerosols, *Atmos. Chem. Phys.*, 13, 3763–3776, doi: 10.5194/acp-13-3763-2013, 2013.



- Kristensen, K., Cui, T., Zhang, H., Gold, A., Glasius, M., and Surratt, J. D.: Dimers in  $\alpha$ -pinene secondary organic aerosol: effect of hydroxyl radical, ozone, relative humidity and aerosol acidity, *Atmos. Chem. Phys.*, 14, 4201–4218, doi:10.5194/acp-14-4201-2014, 2014.
- Kristensen, K., Jensen, L. N., Glasius, M., and Bilde, M.: The effect of sub-zero temperature on the formation and composition of secondary organic aerosol from ozonolysis of alpha-pinene, *Environ. Sci.: Processes and Impacts*, 19, 1220–1234, doi: 10.1039/c7em00231a, 2017.
- Kristensen, K., Jensen, L. N., Quéléver, L. L. J., Christiansen, S., Rosati, B., Elm, J., Teiwes, R., Pedersen, H. B., Glasius, M., Ehn, M., and Bilde, M.: The Aarhus Chamber Campaign on Highly Oxygenated Organic Molecules and Aerosols (ACCHA): particle formation, organic acids, and dimer esters from  $\alpha$ -pinene ozonolysis at different temperatures, *Atmos. Chem. Phys.*, 20, 12549–12567, doi: 10.5194/acp-20-12549-2020, 2020.
- Kumar, M., Busch, D. H., Subramaniam, B., and Thompson, W. H.: Criegee Intermediate Reaction with CO: Mechanism, Barriers, Conformer-Dependence, and Implications for Ozonolysis Chemistry, *J. Phys. Chem. A*, 118, 1887–1894, doi: 10.1021/jp500258h, 2014.
- Kumar, A., Mallick, S., and Kumar, P.: Effect of water on the oxidation of CO by a Criegee intermediate, *Phys. Chem. Chem. Phys.*, 22, 21257–21266, doi: 10.1039/d0cp02682d, 2020.
- Lee, A., Goldstein, A. H., Keywood, M. D., Gao, S., Varutbangkul, V., Bahreini, R., Ng, N. L., Flagan, R. C., and Seinfeld, J. H., Gas-phase products and secondary aerosol yields from the ozonolysis of ten different terpenes, *J. Geophys. Res. Atmos.*, 111, D07302, doi: 10.1029/2005JD006437, 2006.
- Lin, J. J.-M. and Chao, W.: Structure-dependent reactivity of Criegee intermediates studied with spectroscopic methods, *Chem. Soc. Rev.*, 46, 7483–7497, doi: 10.1039/c7cs00336f, 2017.
- Lopez-Hilfiker, F. D., Mohr, C., Ehn, M., Rubach, F., Kleist, E., Wildt, J., Mentel, Th. F., Carrasquillo, A. J., Daumit, K. E., Hunter, J. F., Kroll, J. H., Worsnop, D. R., and Thornton, J. A.: Phase partitioning and volatility of secondary organic aerosol components formed from  $\alpha$ -pinene ozonolysis and OH oxidation: the importance of accretion products and other low volatility compounds, *Atmos. Chem. Phys.*, 15, 7765–7776, doi: 10.5194/acp-15-7765-2015, 2015.
- Ma, Y. and Marston, G.: Multifunctional acid formation from the gas-phase ozonolysis of  $\beta$ -pinene, *Phys. Chem. Chem. Phys.*, 10, 6115–6126, doi: 10.1039/b807863g, 2008.
- Mohr, C., Lopez-Hilfiker, F. D., Yli-Juuti, T., Heitto, A., Lutz, A., Hallquist, M., D'Ambro, E. L., Rissanen, M. P., Hao, L. Q., Schobesberger, S., Kulmala, M., Mauldin III, R. L., Makkonen, U., Sipilä, M., Petäjä, T., and Thornton, J. A.: Ambient observations of dimers from terpene oxidation in the gas phase: Implications for new particle formation and growth, *Geophys. Res. Lett.*, 44, 2958–2966, doi:10.1002/2017GL072718, 2017.
- Müller, L., Reinnig, M.-C., Warnke, J., and Hoffmann, Th.: Unambiguous identification of esters as oligomers in secondary organic aerosol formed from cyclohexene and cyclohexene/ $\alpha$ -pinene ozonolysis, *Atmos. Chem. Phys.*, 8, 1423–1433, doi: 10.5194/acp-8-1423-2008, 2008.
- Naumann, K. H.: COSIMA – a computer program simulating the dynamics of fractal aerosols, *J. Aerosol Sci.*, 34, 1371–1397, 2003.
- Nguyen, T., Peeters, J., and Vereecken, L.: Theoretical study of the gas-phase ozonolysis of  $\beta$ -pinene ( $C_{10}H_{16}$ ), *Phys. Chem. Chem. Phys.*, 11, 5643–5656, doi: 10.1039/b822984h, 2009.
- Onel, L., Lade, R., Mortiboy, J., Blitz, M. A., Seakins, P. W., Heard, D. E., and Stone, D.: Kinetics of the gas phase reaction of the Criegee intermediate  $CH_2OO$  with  $SO_2$  as a function of temperature, *Phys. Chem. Chem. Phys.*, 23, 19415–19423, doi: 10.1039/d1cp02932k, 2021.
- Orlando, J. J. and Tyndall, G. S.: Laboratory studies of organic peroxy radical chemistry: An overview with emphasis on recent issues of atmospheric significance, *Chem. Soc. Rev.*, 41, 6294–6317, doi: 10.1039/c2cs35166h, 2012.



- 580 Pathak, R., Stanier, C. O., Donahue, N. M., and Pandis, S. N.: Ozonolysis of  $\alpha$ -pinene at atmospherically relevant concentrations: Temperature dependence of aerosol mass fractions (yields), *J. Geophys. Res.*, 112, D03201, doi:10.1029/2006JD007436, 2007.
- Pathak, R., Donahue, N. M., and Pandis, S. N.: Ozonolysis of  $\beta$ -pinene: Temperature dependence of secondary organic aerosol mass fraction, *Environ. Sci. Technol.*, 42, 5081–5086, doi: 10.1021/es070721z, 2008.
- 585 Peltola, J., Seal, P., Inkilä, A., and Eskola, A.: Time-resolved, broadband UV-absorption spectrometry measurements of Criegee intermediate kinetics using a new photolytic precursor: unimolecular decomposition of  $\text{CH}_2\text{OO}$  and its reaction with formic acid, *Phys. Chem. Chem. Phys.*, 22, 11797–11808, doi: 10.1039/D0CP00302F, 2020.
- Peng, W. H., Le, C., Porter, W. C., and Cocker III, D. R.: Variability in Aromatic Aerosol Yields under Very Low  $\text{NO}_x$  Conditions at Different  $\text{HO}_2/\text{RO}_2$  Regimes, *Environ. Sci. Technol.*, 56, 750–760, doi: 10.1021/acs.est.1c04392, 2022.
- 590 Percival, C. J., Welz, O., Eskola, A. J., Savee, J. D., Osborn, D. L., Topping, D. O., Lowe, D., Utembe, S. R., Bacak, A., Mcfiggans, G., Cooke, M. C., Xiao, P., Archibald, A. T., Jenkin, M. E., Derwent, R. G., Riipinen, I., Mok, D. W. K., Lee, E. P. F., Dyke, J. M., Taatjes, C. A., and Shallcross, D. E.: Regional and global impacts of Criegee intermediates on atmospheric sulphuric acid concentrations and first steps of aerosol formation, *Faraday Discuss.*, 165, 45–73, doi: 10.1039/c3fd00048f, 2013.
- 595 Porter, W. C., Jimenez, J. L., and Barsanti, K. C.: Quantifying Atmospheric Parameter Ranges for Ambient Secondary Organic Aerosol Formation, *ACS Earth Space Chem.*, 5, 2380–2397, doi: 10.1021/acsearthspacechem.1c00090, 2021.
- Praske, E., Otkjær, R. V., Crounse, J. D., Hethcox, J. C., Stoltz, B. M., Kjaergaard, H. G., and Wennberg, P. O.: Atmospheric autoxidation is increasingly important in urban and suburban North America, *P. Natl. Acad. Sci.*, 115, 64–69, doi: 10.1073/pnas.1715540115, 2018.
- 600 Robinson, C., Onel, L., Newman, J., Lade, R., Au, K., Sheps, L., Heard, D. E., Seakins, P. W., Blitz, M. A., and Stone, D.: Unimolecular Kinetics of Stabilized  $\text{CH}_3\text{CHOO}$  Criegee Intermediates: syn- $\text{CH}_3\text{CHOO}$  Decomposition and anti- $\text{CH}_3\text{CHOO}$  Isomerization, *J. Phys. Chem. A*, 126, 6984–6994, doi: 10.1021/acs.jpca.2c05461, 2022.
- Saathoff, H., Naumann, K.-H., Möhler, O., Jonsson, Å. M., Hallquist, M., Kiendler-Scharr, A., Mentel, Th. F., Tillmann, R., and Schurath, U.: Temperature dependence of yields of secondary organic aerosols from the ozonolysis of  $\alpha$ -pinene and limonene, *Atmos. Chem. Phys.*, 9, 1551–1577, doi: 10.5194/acp-9-1551-2009, 2009.
- 605 Sakamoto, Y., Yajima, R., Inomata, S., and Hirokawa, J.: Water vapour effects on secondary organic aerosol formation in isoprene ozonolysis, *Phys. Chem. Chem. Phys.*, 19, 3165–3175, doi: 10.1039/c6cp04521a, 2017.
- Smith, M. C., Chang, C.-H., Chao, W., Lin, L.-C., Takahashi, K., Boering, K. A., and Lin, J. J.-M.: Strong negative temperature dependence of the simplest Criegee intermediate  $\text{CH}_2\text{OO}$  reaction with water dimer, *J. Phys. Chem. Lett.*, 6, 2708–2713, doi: 10.1021/acs.jpcclett.5b01109, 2015.
- 610 Smith, M. C., Chao, W., Takahashi, K., Boering, K. A., and Lin, J. J.-M.: Unimolecular Decomposition Rate of the Criegee Intermediate  $(\text{CH}_3)_2\text{COO}$  Measured Directly with UV Absorption Spectroscopy, *J. Phys. Chem. A*, 120, 4789–4798, doi: 10.1021/acs.jpca.5b12124, 2016.
- Simon, M., Dada, L., Heinritzi, M., Scholz, W., Stolzenburg, D., Fischer, L., Wagner, A. C., Kürten, A., Rörup, B., He, X.-C., Almeida, J., Baalbaki, R., Baccarini, A., Bauer, P. S., Beck, L., Bergen, A., Bianchi, F., Bräkling, S., Brilke, S., Caudillo, L., Chen, D., Chu, B., Dias, A., Draper, D. C., Duplissy, J., El-Haddad, I., Finkenzeller, H., Frege, C., Gonzalez-Carracedo, L., Gordon, H., Granzin, M., Hakala, J., Hofbauer, V., Hoyle, C. R., Kim, C., Kong, W., Lamkaddam, H., Lee, C. P., Lehtipalo, K., Leiminger, M., Mai, H., Manninen, H. E., Marie, G., Marten, R., Mentler, B., Molteni, U., Nichman, L., Nie, W., Ojdanic, A., Onnela, A., Partoll, E., Petäjä, T., Pfeifer, J., Philippov, M., Quéléver, L. L. J., Ranjithkumar, A., Rissanen, M. P., Schallhart, S., Schobesberger, S., Schuchmann, S., Shen, J., Sipilä, M., Steiner, G., Stozhkov, Y., Tauber, C., Tham, Y. J., Tomé, A. R., Vazquez-Pufleau, M., Vogel, A. L., Wagner, R., Wang, M., Wang, D. S., Wang, Y., Weber, S. K., Wu, Y., Xiao, M., Yan, C., Ye, P., Ye, Q., Zauner-Wieczorek, M., Zhou, X., Baltensperger, U., Dommen, J., Flagan, R. C., Hansel, A., Kulmala, M.,



- Volkamer, R., Winkler, P. M., Worsnop, D. R., Donahue, N. M., Kirkby, J., and Curtius, J.: Molecular understanding of new-particle formation from  $\alpha$ -pinene between  $-50$  and  $+25$  °C, *Atmos. Chem. Phys.*, 20, 9183–9207, doi: 10.5194/acp-20-9183-2020, 2020.
- 625 Sindelarova, K., Granier, C., Bouarar, I., Guenther, A., Tilmes, S., Stavrou, T., Müller, J.-F., Kuhn, U., Stefani, P., and Knorr, W.: Global data set of biogenic VOC emissions calculated by the MEGAN model over the last 30 years, *Atmos. Chem. Phys.*, 14, 9317–9341, doi: 10.5194/acp-14-9317-2014, 2014.
- Valiev, R., Hasan, G., Salo, V.-T., Kubečka, J., and Kurten, T.: Intersystem Crossings Drive Atmospheric Gas-Phase Dimer Formation, *J. Phys. Chem. A*, 123, 6596–6604, doi: 10.1021/acs.jpca.9b02559, 2019.
- 630 Vereecken, L., Rickard, A. R., Newland, M. J., and Bloss, W. J.: Theoretical study of the reactions of Criegee intermediates with ozone, alkylhydroperoxides, and carbon monoxide, *Phys. Chem. Chem. Phys.*, 17, 23847–23858, doi: 10.1039/c5cp03862f, 2015.
- von Hessberg, C., von Hessberg, P., Pöschl, U., Bilde, M., Nielsen, O. J., and Moortgat, G. K.: Temperature and humidity dependence of secondary organic aerosol yield from the ozonolysis of  $\beta$ -pinene, *Atmos. Chem. Phys.*, 9, 3583–3599, doi: 10.5194/acp-9-3583-2009, 2009.
- 635 Wang, P.-B., Truhlar, D. G., Xia, Y., and Long, B.: Temperature-dependent kinetics of the atmospheric reaction between  $\text{CH}_2\text{OO}$  and acetone, *Phys. Chem. Chem. Phys.*, 24, 13066–13073, doi: 10.1039/d2cp01118b, 2022.
- Winterhalter, R., Neeb, P., Grossmann, D., Kolloff, A., Horie, O., and Moortgat, G.: Products and Mechanism of the Gas Phase Reaction of Ozone with  $\beta$ -Pinene, *J. Atmos. Chem.*, 35, 165–197, doi: 10.1023/A:1006257800929, 2000.
- 640 Xu, L., Yang, Z. M., Tsona, N. T., Wang, X. K., George, C., and Du, L.: Anthropogenic–biogenic interactions at night: Enhanced formation of secondary aerosols and particulate nitrogen- And sulfur-containing organics from  $\beta$ -pinene oxidation, *Environ. Sci. Technol.*, 55, 7794–7807, doi: 10.1021/acs.est.0c07879, 2021.
- Yasmeen, F., Vermeylen, R., Szmigielski, R., Inuma, Y., Böge, O., Herrmann, H., Maenhaut, W., and Claeys, M.: Terpenylic acid and related compounds: precursors for dimers in secondary organic aerosol from the ozonolysis of  $\alpha$ - and  $\beta$ -pinene, *Atmos. Chem. Phys.*, 10, 9383–9392, doi: 10.5194/acp-10-9383-2010, 2010.
- 645 Zhang, D. and Zhang, R. Y.: Ozonolysis of  $\alpha$ -pinene and  $\beta$ -pinene: Kinetics and mechanism, *J. Chem. Phys.*, 122, 114308, doi: 10.1063/1.1862616, 2005.
- Zhang, X., McVay, R. C., Huang, D. D., Dalleska, N. F., Aumont, B., Flagan, R., and Seinfeld, J. H.: Formation and evolution of molecular products in  $\alpha$ -pinene secondary organic aerosol, *P. Natl. Acad. Sci.*, 112, 14168–14173, doi: 10.1073/pnas.1517742112, 2015.
- 650 Zhao, Q. L., Liu, F. Y., Wang, W. N., Li, C. Y., Lü, J., and Wang, W. L.: Reactions between hydroxyl-substituted alkylperoxy radicals and Criegee intermediates: correlations of the electronic characteristics of methyl substituents and the reactivity, *Phys. Chem. Chem. Phys.*, 19, 15073–15083, doi: 10.1039/c7cp00869d, 2017.
- 655 Zhao, Y., Thornton, J. A., and Pye, H. O. T.: Quantitative constraints on autoxidation and dimer formation from direct probing of monoterpene-derived peroxy radical chemistry, *P. Natl. Acad. Sci.*, 115, 12142–12147, doi: 10.1073/pnas.1812147115, 2018.

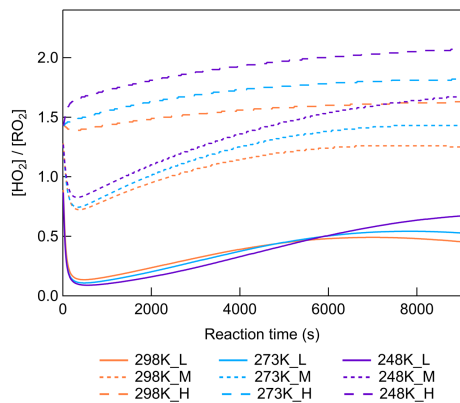




660 **Table 1. Summary of experimental conditions.**

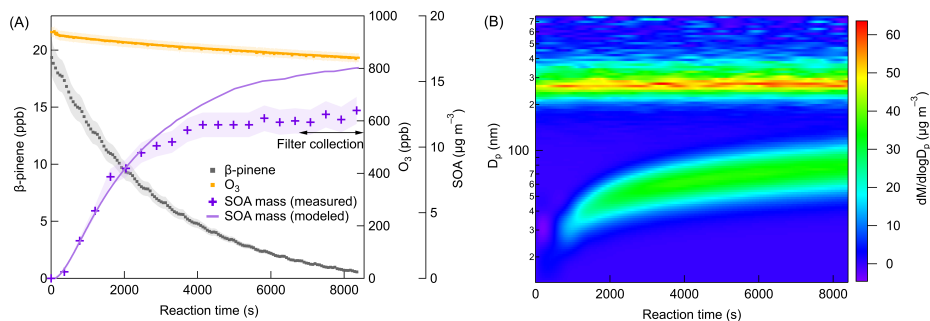
Exp.	$\beta$ -pinene (ppb)	O <sub>3</sub> (ppm)	CO (ppm)*	Formic acid (ppb)	T (K)	RH (%)	[HO <sub>2</sub> ]/[RO <sub>2</sub> ]
298a	19.3±1.2	0.93±0.05	25	0	298±0.3	< 0.1	L (low)
298b	19.3±1.2	0.93±0.05	100	0	298±0.3	< 0.1	M (middle)
298c	19.3±1.2	0.93±0.05	400	0	298±0.3	< 0.1	H (high)
298d	19.3±1.2	0.93±0.05	25	90±10	298±0.3	< 0.1	L
298e	19.3±1.2	0.93±0.05	100	90±10	298±0.3	< 0.1	M
298f	19.3±1.2	0.93±0.05	25	0	298±0.3	14.7±1.2	L
273a	18.2±1.0	1.10±0.05	23	0	273±0.3	< 0.1	L
273b	18.2±1.0	1.10±0.05	92	0	273±0.3	< 0.1	M
273c	18.2±1.0	1.10±0.05	366	0	273±0.3	< 0.1	H
273d	18.2±1.0	1.10±0.05	23	90±10	273±0.3	< 0.1	L
273e	18.2±1.0	1.10±0.05	92	90±10	273±0.3	< 0.1	M
273f	18.2±1.0	1.10±0.05	23	0	273±0.3	81.3±1.0	L
248a	16.3±0.8	1.30±0.05	21	0	248±0.3	< 0.1	L
248b	16.3±0.8	1.30±0.05	84	0	248±0.3	< 0.1	M
248c	16.3±0.8	1.30±0.05	333	0	248±0.3	< 0.1	H
248d	16.3±0.8	1.30±0.05	21	90±10	248±0.3	< 0.1	L
248e	16.3±0.8	1.30±0.05	84	90±10	248±0.3	< 0.1	M
248f	16.3±0.8	1.30±0.05	21	0	248±0.3	70.5±1.8	L

\* Uncertainty of 5%.



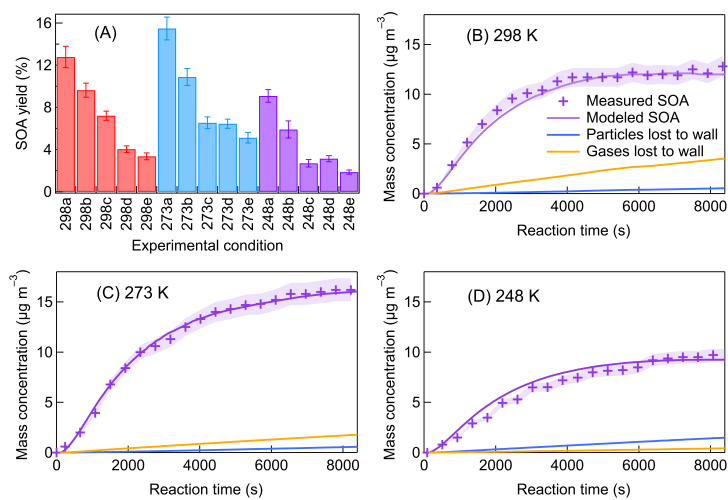
665

Figure 1. Simulated  $[HO_2]/[RO_2]$  as a function of reaction time at different  $[HO_2]/[RO_2]$  conditions and different temperatures (Exp. 298abc, 273abc, 248abc).



670

Figure 2. Time series of (A)  $\beta$ -pinene mixing ratio,  $O_3$  mixing ratio, measured SOA mass concentrations, and simulated SOA mass concentrations after wall loss correction (B) Particle mass size distributions ( $dM/d\log D_p$ ) at 298 K (Exp. 298a).



675

**Figure 3.** (A) SOA yields at different experimental conditions (a–c: increasing  $[HO_2]/[RO_2]$ ; d, e: scavenging SCIs). Measured and modeled SOA mass concentrations, and the wall losses of particles and gases at (B) 298 K (C) 273 K (D) 248 K (Exp. 298a, 273a, 248a).



680

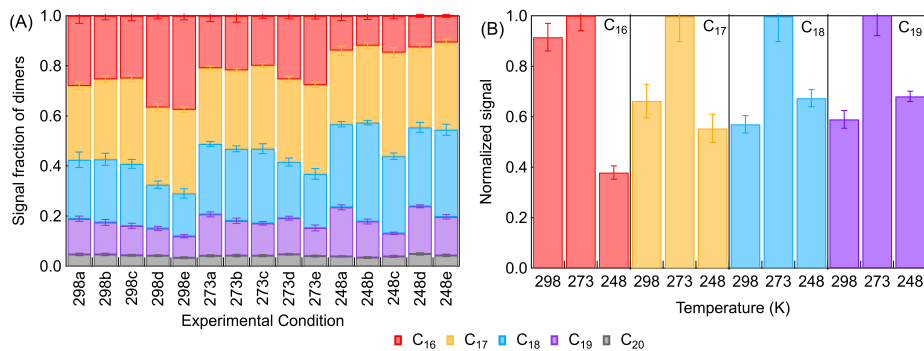


**Figure 4. (A) Fractions of different dimer species of all particle-phase dimers (a–c: increasing  $[HO_2]/[RO_2]$ ; d, e: scavenging SCIs). (B) Temperature dependence of the relative abundance of different dimers (Exp. 298a, 273a, 248a).**



685

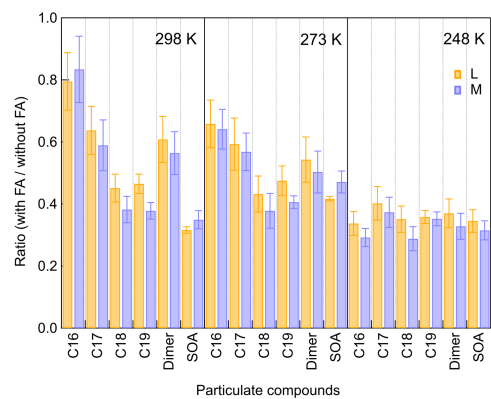


**Figure 5.** The relative changes of particulate dimers and SOA yields after scavenging SCIs at low (L) and middle (M)  $[HO_2]/[RO_2]$  (Exp. 298de, 273de, 248de).





690

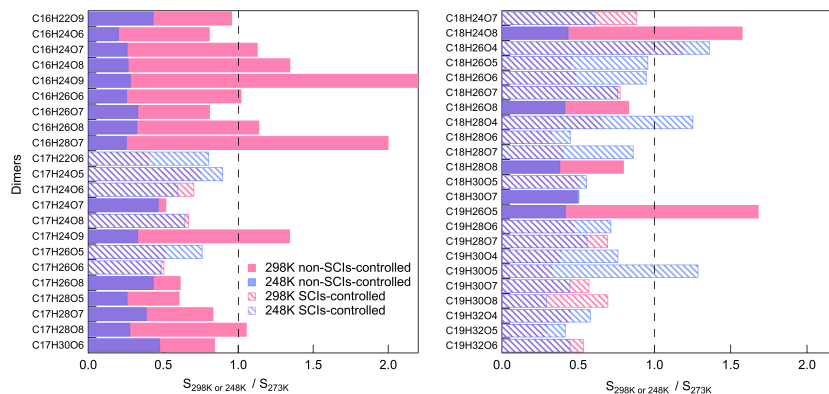
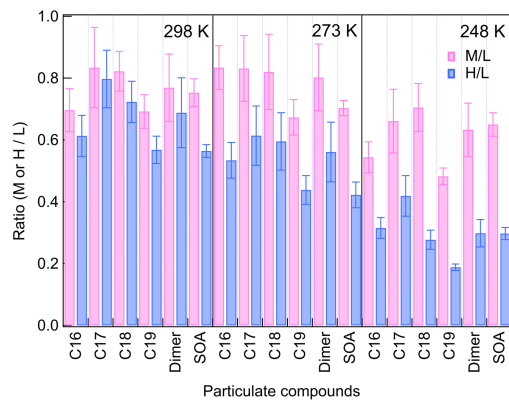


Figure 6. The relative changes of SCIs-controlled and non-SCIs-controlled abundant dimers at 298 K or 248 K versus 273 K (The relative standard deviations are within 25 %).



695



**Figure 7.** The relative changes of particulate dimers and SOA yields at middle (M) and high (H)  $[HO_2]/[RO_2]$  compared to low (L)  $[HO_2]/[RO_2]$  (Exp. 298abc, 273abc, 248abc).



700

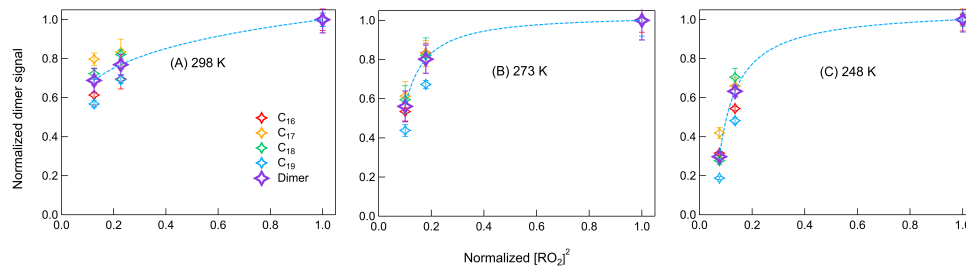


**Figure 8.** Correlation between normalized dimer signals and normalized  $[RO_2]^2$  at (A) 298 K (B) 273 K (C) 248 K (Exp. 298abc, 273abc, 248abc). The dashed lines represent the changing tendency of dimers.



705

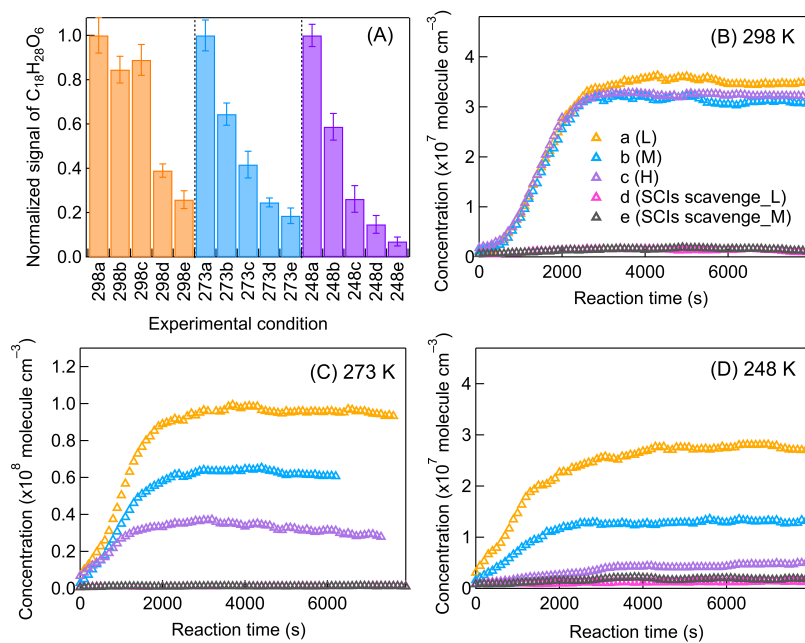


**Figure 9.** The impact of  $[\text{HO}_2]/[\text{RO}_2]$  and SCIs scavenging on (A) the total  $\text{C}_{18}\text{H}_{28}\text{O}_6$  signal in both the gas and particle phase (normalized to the largest signal at each temperature), and the gas-phase variation of  $\text{C}_{18}\text{H}_{28}\text{O}_6$  at (B) 298 K (C) 273 K (D) 248 K (a–c: increasing  $[\text{HO}_2]/[\text{RO}_2]$ ; d, e: scavenging SCIs).

710

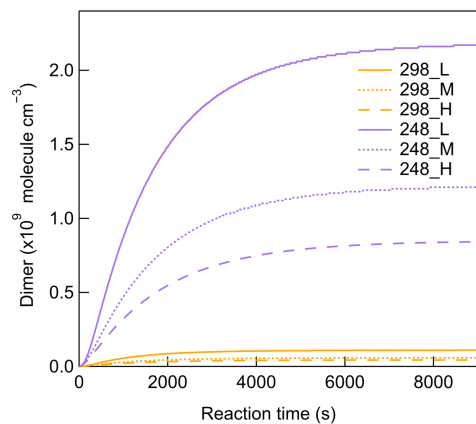


**Figure 10.** Simulated dimers formation from reaction of C<sub>9</sub>-SCIs with RO<sub>2</sub> radicals at different [HO<sub>2</sub>]/[RO<sub>2</sub>] conditions for 298 K and 248 K.

715